science.sciencemag.org/content/369/6503/eaba3373/suppl/DC1

Supplementary Material for

Structural insights into differences in G protein activation by family A and family B GPCRs

Daniel Hilger, Kaavya Krishna Kumar, Hongli Hu, Mie Fabricius Pedersen, Evan S. O'Brien, Lise Giehm, Christine Jennings, Gözde Eskici, Asuka Inoue, Michael Lerch, Jesper Mosolff Mathiesen*, Georgios Skiniotis*, Brian K. Kobilka*

*Corresponding author. Email: jmm@zealandpharma.com (J.M.M.); yiorgo@stanford.edu (G.S.); kobilka@stanford.edu (B.K.K)

Published 31 July 2020, *Science* **369**, eaba3373 (2020)
DOI: 10.1126/science.aba3373

This PDF file includes:

Supplementary Materials

Fig. S1 – S9

Table S1 – S9

References 51 - 73

Supplemental Figures

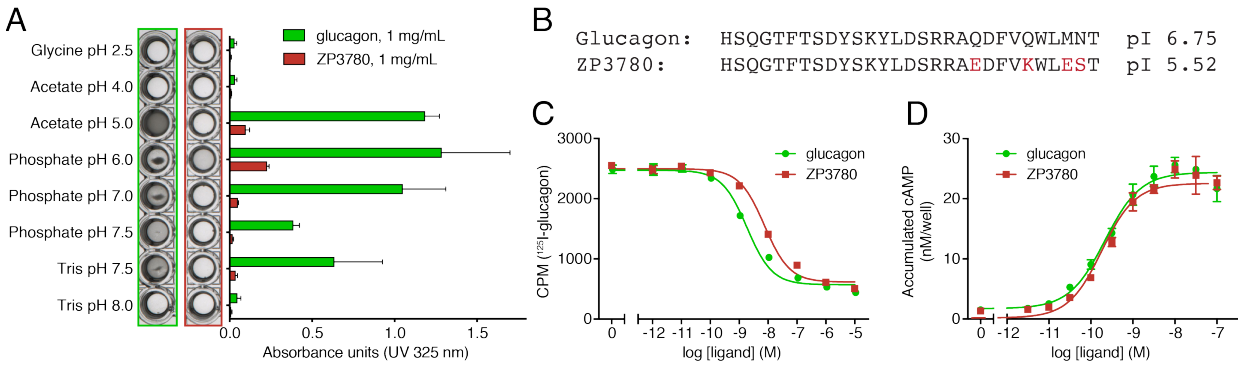

Fig. S1: *In vitro* properties of ZP3780 compared to glucagon.
(A) The improved solubility of ZP3780 (red) compared to glucagon (green) in a large range of buffers and pH, also around pH 7.5 as observed and measured by UV 325 nm absorbance. **(B)** Sequence of glucagon and ZP3780 with the mutations in ZP3780 highlighted in red. **(C)** ZP3780 (red) displaces [^{125}I]-glucagon to non-specific levels as observed for glucagon (green) in competition binding studies with GCGR overexpressed in HEK293 cell membranes. **(D)** ZP3780 (red) has a similar potency and E_{max} as glucagon (green) in a functional cAMP accumulation assay in HEK293 cells transiently expressing the GCGR. The affinity of ZP3780 (C) is marginally lower than glucagon (also refer to Tables S3 and S4). Data represent mean ± s.e.m. from three (A) or four (C and D) independent experiments.

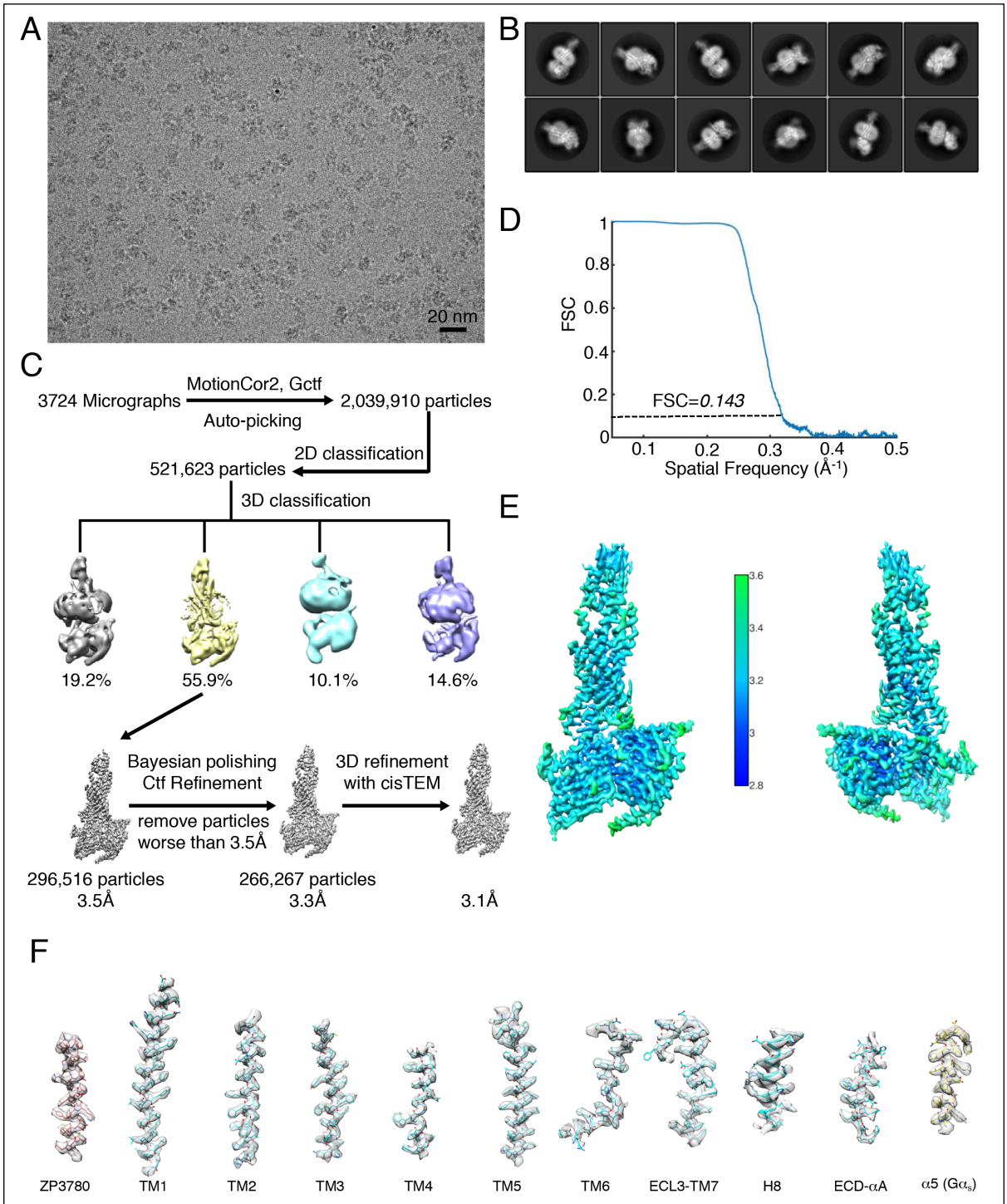

Fig. S2: Cryo-EM data processing.

(A) Representative cryo-EM image of the GCGR-G_s complex. Scale bar: 20 nm. **(B)** Representative reference-free 2D cryo-EM averages of GCGR-G_s. **(C)** Cryo-EM data processing flow chart of GCGR, including particle selection, classifications and density map reconstruction. **(D)** 'Gold standard' FSC curves from RELION (*55*) indicate that the map for the GCGR-G_s complex reaches a nominal resolution of 3.1Å at FSC = 0.143. **(E)** Three-dimensional density maps of the GCGR-G_s complex, colored by local resolution. **(F)** Cryo-EM density map and model are shown for ZP3780, all seven transmembrane α-helices, ICL3, and αA (ECD) of GCGR and α5 of $G\alpha_s$.

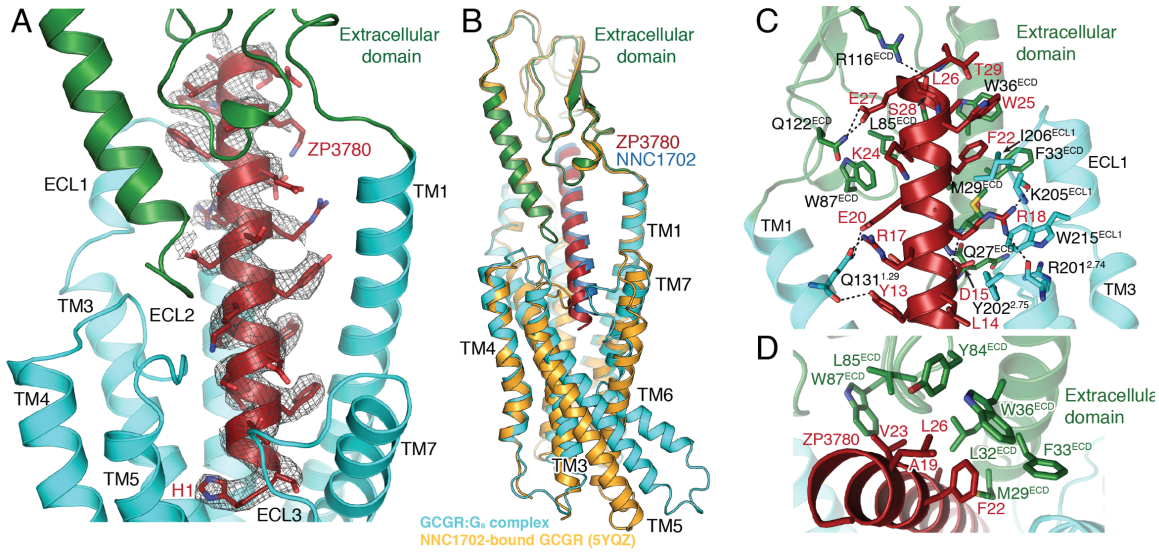

Fig. S3: Interactions between the full agonist ZP3780 and GCGR.
(A) The cryo-EM density (displayed as a mesh) of the bound ZP3780 (red) in the peptide binding pocket of GCGR (TMs shown in cyan and the extracellular domain (ECD) shown in green). **(B)** Comparison of peptide-binding mode of full-agonist ZP3780 (red)-bound GCGR (cyan) and partial agonist-bound NNC1702 (blue)-bound GCGR (orange) (PDB 5YQZ) (*17*). **(C)** The C terminus of ZP3780 (red) engages residues in polar (dotted lines) and hydrophobic (residues shown) interactions with the ECD (green), TMs 1, 2, 3, and ECL1 (cyan). **(D)** Hydrophobic interaction between residues in ZP3780 (red) and the ECD of GCGR (green).

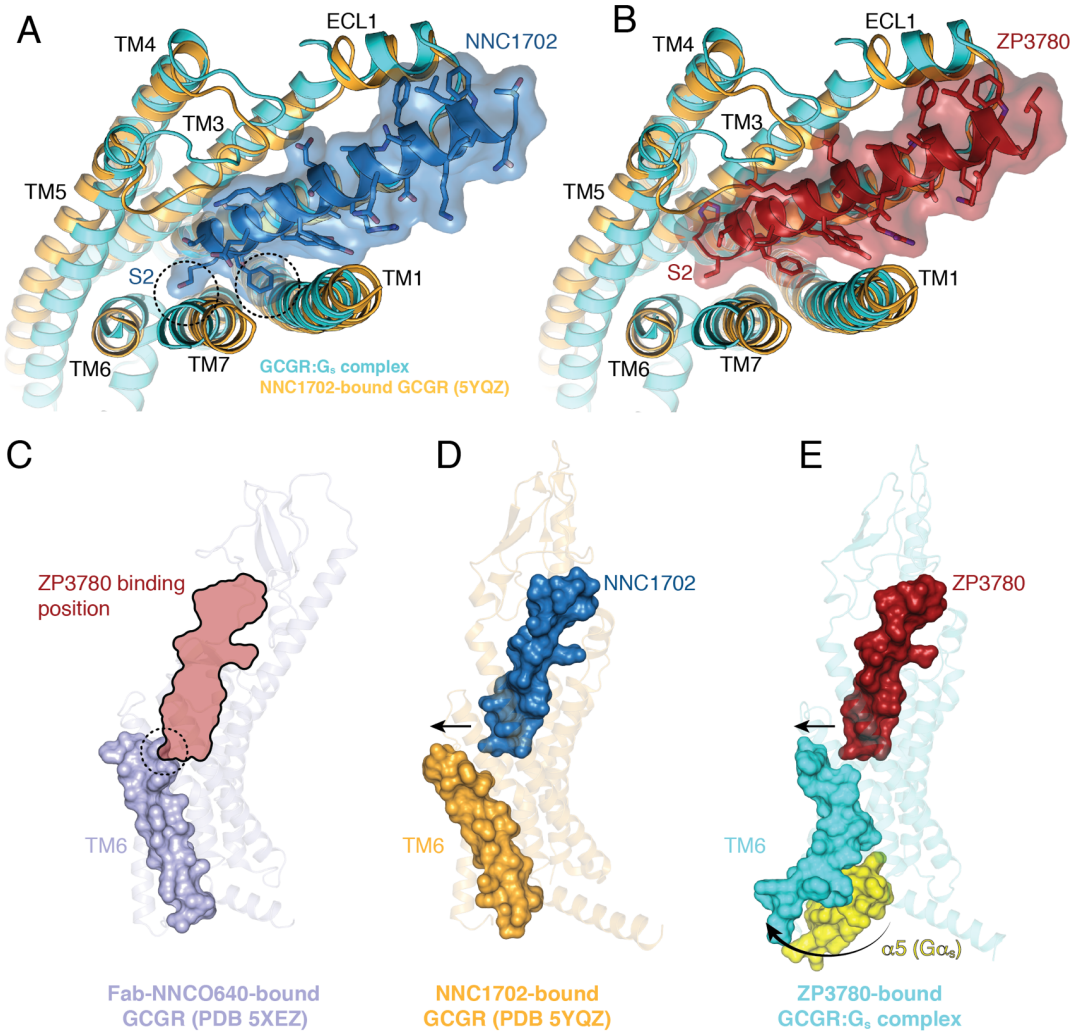

Fig. S4: Peptide and G protein-induced conformational changes in transmembrane domain 6 of GCGR.

Comparison of the ligand binding mode of NNC1702 **(A)** and ZP3780 **(B)**. The N terminus of the partial agonist NNC1702 (blue), which lacks H1 and has a D9E mutation in comparison to the WT glucagon, binds closer to TM7 than the full agonist ZP3780 (red). While the inactive peptide-bound state of GCGR (yellow) (PDB 5YQZ) is compatible with binding of NNC1702, NNC1702 binding to the active conformation of GCGR (cyan) would lead to steric clashes of S2 and F6 with TM7 and TM1, respectively (highlighted with a dashed circles). The residues H1 and D9 of ZP3780 seem to cause the peptide to bind closer to TM3, which releases potential clashes and allows formation of the active conformation of TM1 and TM7 as seen in the GCGR-G_s complex structure. **(C)** The binding position of ZP3780 (black outline based on the ZP3780-bound GCGR-G_s complex structure (E)) overlaps with the C-terminal end of TM6 (highlighted with a dashed circle) in the Fab-bound inactive structure of GCGR (PDB 5XEZ, Fab and NNCO640 are not shown for clarity). **(D)** The extracellular tip of TM6 (orange) moves outward to accommodate NNC1702 (blue) binding in the partial agonist-bound GCGR structure (PDB 5YQZ). **(E)** In the GCGR-G_s complex structure (cyan), the N and C termini of TM6 move away from the receptor core to accommodate ZP3780 (red) and the C-terminal α5 helix of $G\alpha_s$ (yellow), respectively. The necessity for the outward movement of both the extracellular and intracellular sides of TM6 to allow binding of the bulky peptide and G protein might result in the extreme kink formation in family B GPCRs.

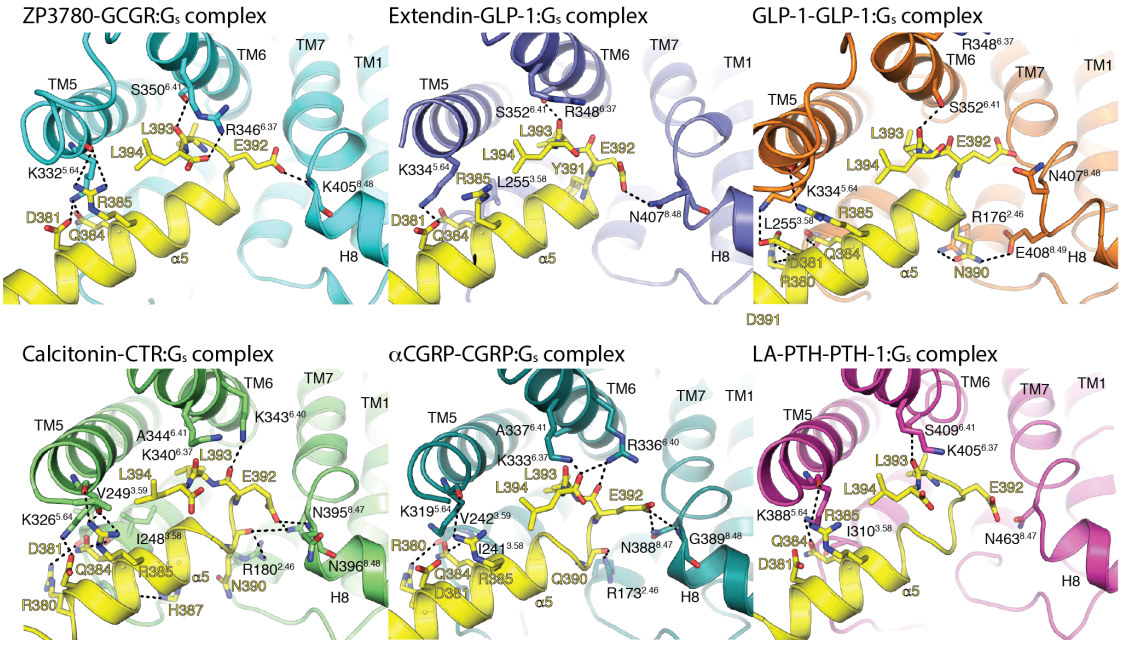

Fig. S5: Comparison of the C-terminal α5 helix binding mode of Gα$_s$ in family B GPCRs.

Cytoplasmic views of the GCGR (cyan) with the C-terminal α5 helix of Gα$_s$ (yellow), compared to the Extendin-GLP-1R-G$_s$ complex (purple, PDB 6B3J), GLP-1-GLP-1R-G$_s$ complex (orange, PDB 5VAI), Calcitonin-CTR-G$_s$ complex (green, PDB 6NIY), αCGRP-CGRP-G$_s$ complex (deep teal, PDB 6E3Y), and the LA-PTH-PTH1R-G$_s$ complex (pink, PDB 6NBF). H-bonds are shown as black dashed lines.

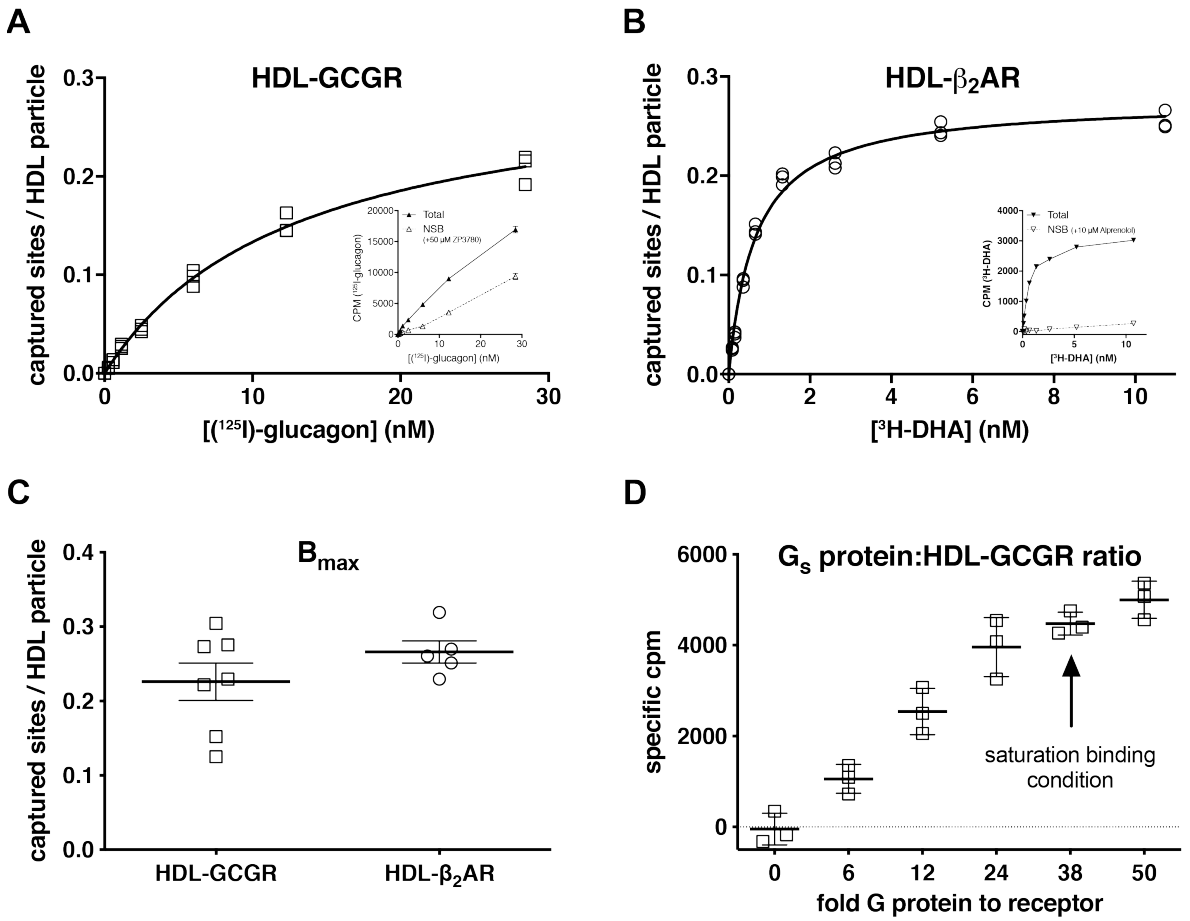

Fig. S6: Radioligand saturation binding to HDL-reconstituted (A) GCGR and (B) β2AR. (C) The B_{max} values of the reconstituted GCGR and β_2AR, given as the ratio of captured sites (i.e. detectable sites) per reconstituted GCGR or β_2AR HDL particle, are similar and not significantly different when compared in an unpaired *t*-test, $p = 0.2473$ (two-tailed *p*-value, Table S8). **(D)** The HDL-GCGR required presence of G_s to obtain detectable [^{125}I]-glucagon binding to the receptor. Data shown in (A) and (B) are representative experiments from 7 or 5 independent experiments, respectively, performed with similar results and summarized in C where data is given as mean ± s.e.m. Data in (D) are given as mean ± SD from a representative experiment performed in triplicate and repeated in 3 independent experiments with similar results.

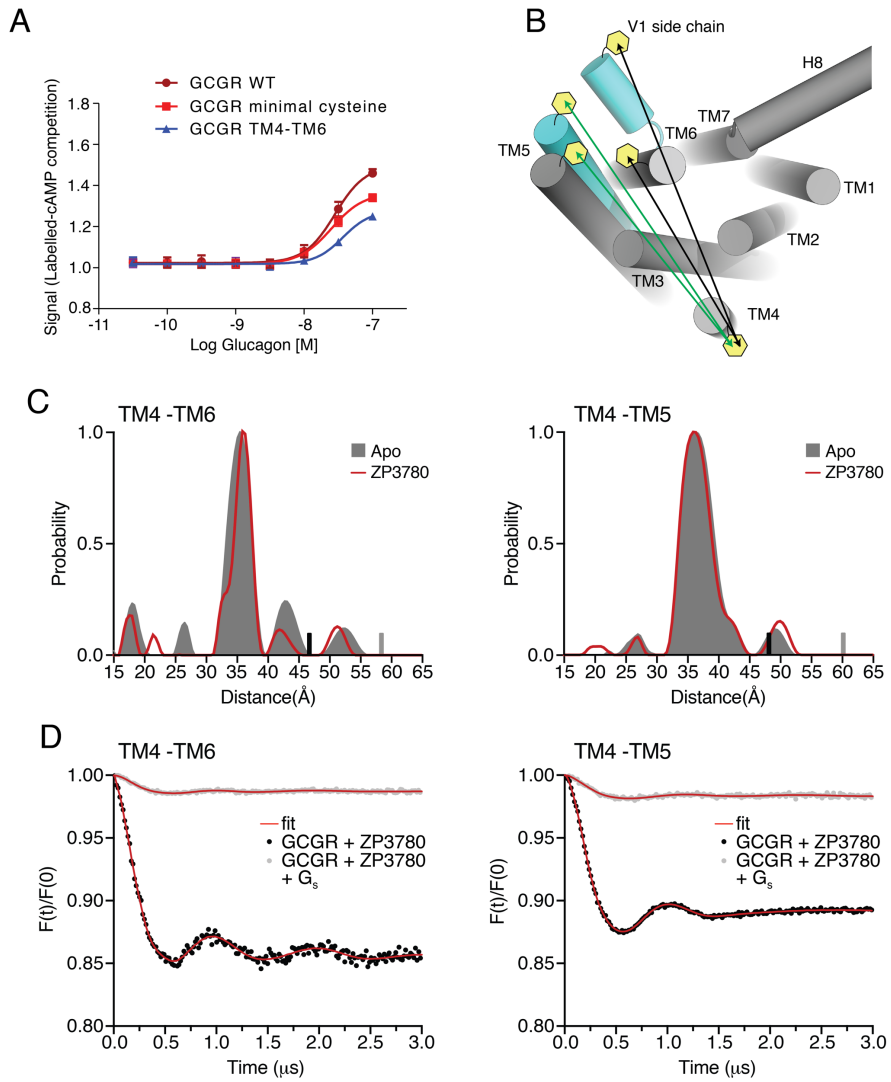

Fig. S7: Characterization of minimal cysteine constructs of GCGR and DEER data. **(A)** cAMP assay showing -log EC_{50} values for WT, minimal cysteine and TM4/TM6 constructs of GCGR. **(B)** Intracellular GCGR spin-labeling allows the detection of ZP3780-dependent DEER distance changes, as schematically shown for the TM4-TM5 and TM4-TM6 double cysteine pairs. **(C)** Comparison of DEER distance distributions between spin labels attached to TM4 and TM6 (left) and TM4 and TM5 (right) of GCGR in the apo (grey filled) and ZP3780-bound (red) state. The upper limit of reliable distance (*r*) and width (σ) determination are shown as grey and black bars, respectively. **(D)** Normalized, background-corrected dipolar evolutions of spin-labeled ZP3780-bound GCGR before (black dots) and after addition of G_s (grey dots) in reducing agent-free buffer. The G_s-dependent decrease in modulation depth, observed for both double cysteine pairs TM4-TM6 (left) and TM4-TM5 (right), indicates spin label dissociation from the receptor upon interaction with the G protein.

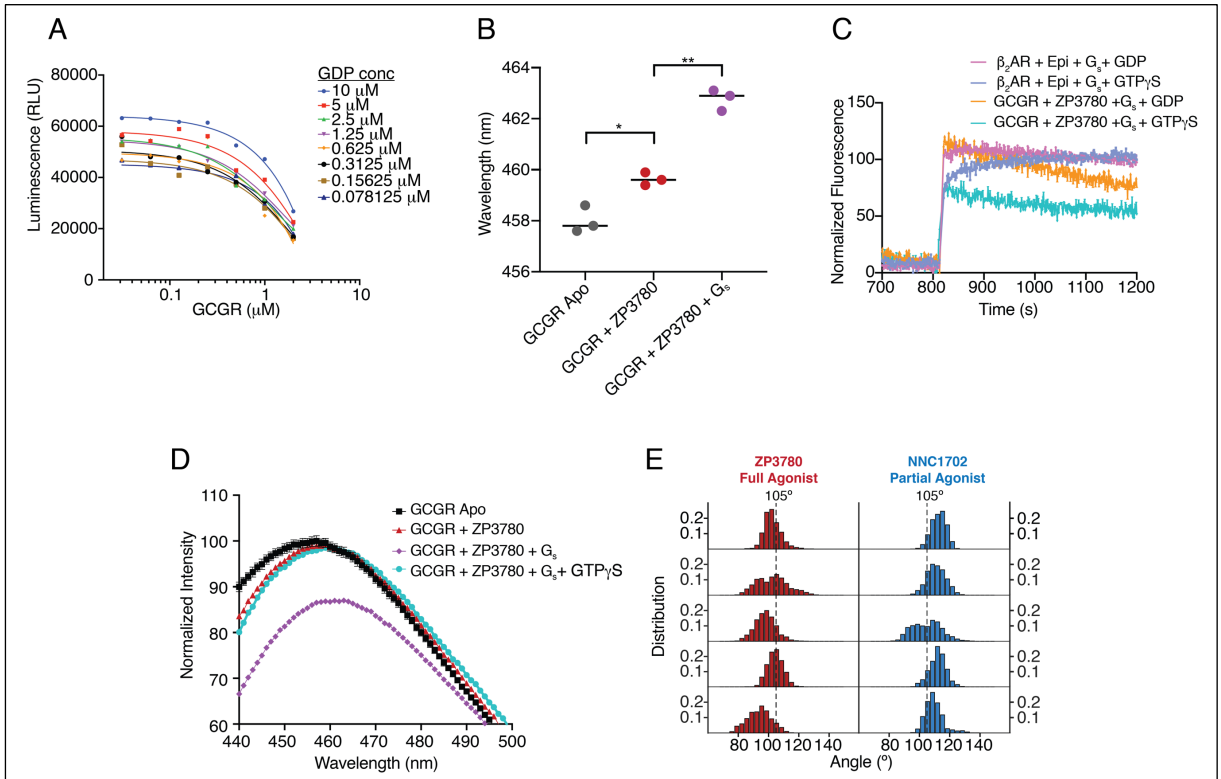

Fig. S8: Effect of ligand and nucleotide on GCGR and G_s activation.

(A) Effect of GDP on GCGR-induced G_s activation. In the presence of GCGR, increasing GDP concentration decreases GTP turnover in the *Glo-assay*, which is compensated by increasing receptor concentrations. **(B)** The difference in the λ_{max} value between Apo and ZP3780-bound, bimane-labeled GCGR (TM6) is statistically significant (*, $p = 0.019$), as is the λ_{max} value of ZP3780-bound and ZP3780 + G_s bound GCGR (**, $p = 0.001$). **(C)** In a FRET association assay with Cy3B-labeled receptors and Sulfo-Cyanine 5-labeled G_s, addition of nucleotide, GDP or GTPγS results in dissociation of G_s from the receptors. GCGR (GDP: orange, GTPγS: teal) and β_2AR (GDP: pink, GTPγS: purple). **(D)** The fluorescence intensity of bimane-labeled GCGR (TM6) bound to ZP3780 and coupled to G_s (purple curve) increases after an 1-hour incubation of the complex with GTPγS (cyan) to the level of ZP3780-bound GCGR in the absence of G protein (red). (E) MD simulations of GCGR (after G_s removal) showing the distribution of the angle between residues V368-G359-K344 of TM6. In the presence of ZP3780 (full agonist, red) TM6 remains more outward than in the presence of NNC1702 (partial agonist, blue). Shown are the plots of the angle distributions calculated for five independent simulations for each ligand condition.

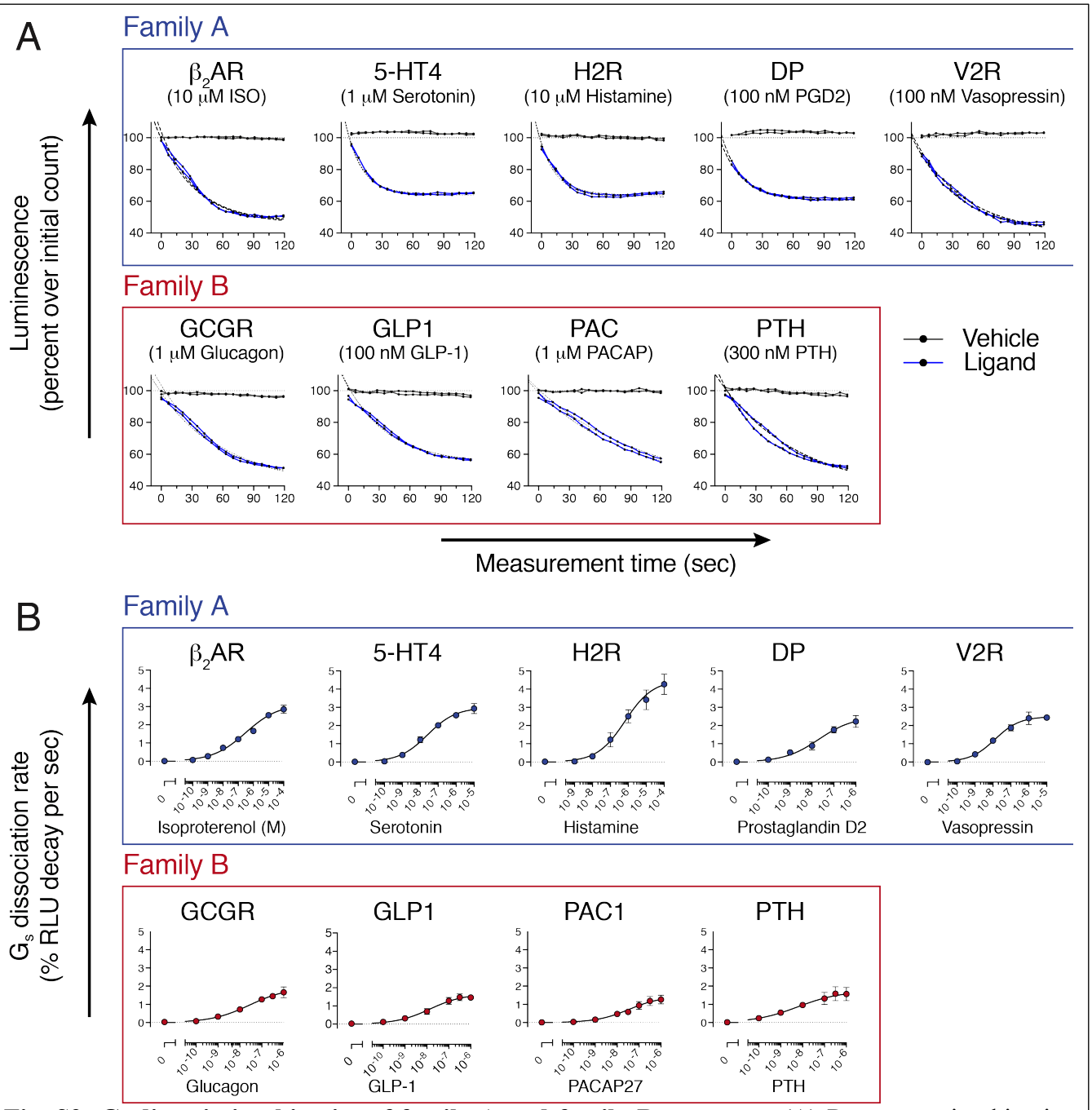

Fig. S9: G_s dissociation kinetics of family A and family B receptors. (A) Representative kinetics data for GPCR ligand-induced G_s dissociation. HEK293 cells expressing the NanoBiT-G_s protein and an indicated GPCR, which was optimized to express equally among the tested GPCRs, were loaded with coelenterazine, a luciferase substrate. After measurement of initial luminescent signals, vehicle or an indicated concentration of a ligand was manually added to the cells and from thereon luminescent signals were recorded continuously with a luminescent microplate reader at intervals of 7 sec. Dashed lines represent one-phase decay curves that were fit to the ligand-treated data points. Data shown are a representative of at least three independent experiments with each performed in duplicate. **(B)** Concentration-response curves for G_s dissociation rates. HEK293 cells expressing the NanoBiT-G_s protein and an indicated GPCR were treated with titrated concentration of a test ligand and, for each concentration, a G_s dissociation rate was calculated by fitting a one-phase decay curve. Concentration-response plots were fitted to a sigmoidal curve, from which maximum G_s dissociation rate (E_{max}) was calculated and shown (Fig. 7). Symbols and error bars represent mean and s.e.m. of 3-7 independent experiments (see Table S8 for details).

Supplemental Tables

Table S1: Solubility of glucagon and ZP3780 at different pH values.

Buffer	Glucagon	ZP3780
Acetate pH 4	>1 mg ml^{-1}	>1 mg ml^{-1}
Acetate pH 5	>1 mg ml^{-1}	>1 mg ml^{-1}
Phosphate pH 6	<0.5 mg ml^{-1}	>1 mg ml^{-1}
Phosphate pH 7	<0.5 mg ml^{-1}	>1 mg ml^{-1}
Phosphate pH 7.5	<0.5 mg ml^{-1}	>5 mg ml^{-1}
Tris pH 7.5	<0.5 mg ml^{-1}	>1 mg ml^{-1}
Tris pH 8	Not tested	>1 mg ml^{-1}
Glycine pH 9	Not tested	>1 mg ml^{-1}

Table S2: Comparison of the fibrillation of glucagon and ZP3780.

	Fibrillation	
	Aggregation lag time by ThT	
	Glucagon	ZP3780
	pH 2.5	pH 7.5
No Agitation	13.1 ± 1.0 hr	No fibrillation
Agitation	1.8 ± 0.2 hr	19.6 ± 0.5 hr

[a]The fibrillation tendency was investigated using the fluorescent probe Thioflavin T (ThT), which detects the presence of amyloid fibrils.
[b]The aggregation propensity was accelerated using high temperature (40°C) combined with or without agitation.

Table S3: Comparison of the binding affinity of glucagon and ZP3780.

	K_i (nM)	pK_i ± SEM	*p*-value	n
Glucagon	1.7	8.76 ± 0.06		4
ZP3780	6.9	8.16 ± 0.04	<0.0001	4

[a]pK_i values were determined by the Cheng-Prussov equation after non-linear regression of data to single binding site model.
[b]Average K_i-values was calculated from the pK_i.
[c]Data are given as mean ± s.e.m. from 4 independent experiments performed in duplicate or triplicate. Statistics was performed as an extra sum-of-squares *F* test.

Table S4: Comparison of the EC_{50} and E_{max} values of glucagon an ZP3780 in GCGR-mediated cAMP signaling assays.

	EC_{50} (nM)	**pEC_{50} ± SEM**	**p-value**	**E_{max} (nM cAMP) ± SEM**	***p*-value**	**n**
Glucagon	0.23	9.64 ± 0.03		23.4 ± 0.8		4
ZP3780	0.33	9.49 ± 0.06	0.2237	23.0 ± 1.6	0.5929	4

[a]pEC_{50} and E_{max} values were determined by fitting data to a four-parameter dose-response curve.
[b]Hill slopes were 1.0 and 1.2 for glucagon and ZP3780, respectively, and not statistically different (extra sum-of-squares *F* test, $p = 0.7892$).
[c]Average EC_{50}-value was calculated from the pEC_{50}. E_{max} was measured as nM cAMP pr. well.
[d]Data are given as mean ± s.e.m. from 4 independent experiments performed in duplicate.
[e]Statistics were performed as extra sum-of-squares *F* tests.

Table S5: Data collection, model refinement and validation.

Data Collection	
Voltage (kX)	300
Magnification	47,169
Total electron dose ($e^-/Å^2$)	50
Defocus range (μm)	1.2-2.2
Calibrated pixel size (Å)	1.06
Micrograph collected (no.)	3,724
Data processing	
Extracted particles (no.)	2,039,910
Particles used for final reconstruction (no.)	296,516
Final map resolution (Å, 0.143 FSC)	3.1
Map resolution range (Å)	2.8-3.6
Map sharpening B factor (Å2)	Pre -90, post -30
Model content	
Initial models used (PBD code)	5YQZ (GCGR), 5VAI (G_s/Nb35)
Total number of atoms	9,262
No. of protein residues	1,176
No. of ligands	0
Model validation	
CC map vs. model (%)	80
RMSD	
Bond lengths (Å) / Bond angles (°)	0.007/0.942
Ramachandran plot statistics	
Most favored (%)	94.13
Outliers (%)	0
Rotamer outliers (%)	0
C-beta deviations	0
Clash score	6.18

Table S6: **cAMP accumulation assay for GCGR mutants and surface expression of GCGR mutants analyzed by cell surface ELISA.**

GCGR	EC_{50} (nM)	pEC_{50} ± SEM	*p*-value to WT	E_{max} (% WT) ± SEM	*p*-value to WT	n	Surface expr. (% WT) ± SEM	*p*-value (to WT)	n
WT	0.14	9.87 ± 0.11		106 ± 3		8	96 ± 3		6
Q232A	51	7.30 ± 0.07	<0.0001	92 ± 3	0.0407	6	101 ± 10	0.9932 (ns)	6
L242A	3	8.56 ± 0.19	<0.0001	77 ± 5	0.0006	3	96 ± 8	>0.9999 (ns)	3
F322A	111	6.95 ± 0.17	<0.0001	84 ± 8	0.0065	3	78 ± 6	0.3072 (ns)	3
D370A	>100	n.d	n.d	>74	n.d	3	108 ± 6	0.7609 (ns)	3
R378A	n.d	n.d	n.d	n.d	n.d	3	103 ± 10	0.9761 (ns)	3
D385A	>100	n.d	n.d	>69	n.d	6	82 ± 3	0.4097 (ns)	6
L395A	0.82	9.09 ± 0.19	0.0036	72 ± 4	<0.0001	3	82 ± 9	0.6015 (ns)	3
Y400F	0.28	9.55 ± 0.22	0.4126 (ns)	60 ± 3	<0.0001	3	78 ± 3	0.3638 (ns)	3
Mock							6 ± 0.3	<0.0001	6

[a]pEC_{50} and E_{max} values were determined by fitting data to a three-parameter dose-response curve. Average EC_{50}-values were calculated from the pEC_{50}. E_{max} values were normalized to that of WT in each of the independent experiments.
[b]Data are given as mean ± s.e.m. from the indicated number of independent experiments performed in triplicate n.d, not determined, as parameter could not be reliably fitted.
[c]Statistics were performed by one-way ANOVA, followed by Dunnett's multiple comparisons test to the WT. Each *p*-value was adjusted to account for multiple comparisons. ns, not significant

Table S7: **Comparison of G_s association and nucleotide binding and release rates between GCGR and β_2AR.**

	GCGR	β_2AR	*p*-value	n
Max. GTP-turnover rate ($GTP\ min^{-1}\ G_s^{-1}$)	0.1112 ± 0.0019	7.875 ± 0.1863	<0.0001	9
FRET association ($k_{on}\ s^{-1}$)	0.0044 ± 0.0002	0.0077 ± 0.0006	0.0004	6
GDP release ($k_{off}\ s^{-1}$)	0.0022 ± 0.0002	0.042 ± 0.0077	0.0065	3
BODIPY-FL-GTPγS binding ($k_{on}\ s^{-1}$)	0.00100 ± 0.00005	0.00296 ± 0.0002	0.0008	3

[a]Data are given as mean ± s.e.m from 3 or 9 independent experiments as indicated.
[b]Statistics were performed as Unpaired *t*-test.

Table S8: Statistics for the determination of B_{max} values from radioligand saturation binding experiments on β_2AR-HDL and GCGR-HDL particles.

	B_{max} ± SEM	K_d ± SEM	n
GCGR-HDL	0.23 ± 0.03	11.7 ± 2.2	7
β_2AR-HDL	0.27 ± 0.01	1.1 ± 0.2	5
Unpaired *t*-test			
two tailed *p*-value	0.2473 (ns)		

[a]B_{max} values were compared in an unpaired *t*-test, and the two-tailed *p*-value given.
[b]Data are given as mean ± s.e.m from 7 or 5 independent experiments as indicated.

Table S9: **Comparison of G_s dissociation rates and surface expression of different family A and family B GPCRs.**

		G_s Dissociation (% RLU change per sec)		Surface expression (% β_2AR MFI)	
		Mean ± SEM	**n**	**Mean ± SEM**	**n**
family A	β_2AR	3.24 ± 0.33	5	100	8
	5-HT4	3.07 ± 0.37	5	92.2 ± 4.7	4
	DP	2.39 ± 0.32	5	99.3 ± 3.7	7
	H2R	4.65 ± 0.56	4	111.2 ± 5.5	5
	V2R	2.50 ± 0.12	5	73.8 ± 5.5	4
family B	GCGR	2.01 ± 0.35	5	99.8 ± 4.9	4
	GLP1	1.74 ± 0.13	5	84.8 ± 5.1	3
	PAC1	1.40 ± 0.28	5	102.7 ± 6.5	7
	PTH	1.62 ± 0.37	5	109.6 ± 4.9	3

References and Notes

1. Y.-L. Liang, M. Khoshouei, G. Deganutti, A. Glukhova, C. Koole, T. S. Peat, M. Radjainia, J. M. Plitzko, W. Baumeister, L. J. Miller, D. L. Hay, A. Christopoulos, C. A. Reynolds, D. Wootten, P. M. Sexton, Cryo-EM structure of the active, G_s-protein complexed, human CGRP receptor. *Nature* **561**, 492–497 (2018). doi:10.1038/s41586-018-0535-y Medline

2. Y.-L. Liang, M. Khoshouei, A. Glukhova, S. G. B. Furness, P. Zhao, L. Clydesdale, C. Koole, T. T. Truong, D. M. Thal, S. Lei, M. Radjainia, R. Danev, W. Baumeister, M.-W. Wang, L. J. Miller, A. Christopoulos, P. M. Sexton, D. Wootten, Phase-plate cryo-EM structure of a biased agonist-bound human GLP-1 receptor-Gs complex. *Nature* **555**, 121–125 (2018). doi:10.1038/nature25773 Medline

3. Y.-L. Liang, M. Khoshouei, M. Radjainia, Y. Zhang, A. Glukhova, J. Tarrasch, D. M. Thal, S. G. B. Furness, G. Christopoulos, T. Coudrat, R. Danev, W. Baumeister, L. J. Miller, A. Christopoulos, B. K. Kobilka, D. Wootten, G. Skiniotis, P. M. Sexton, Phase-plate cryo-EM structure of a class B GPCR-G-protein complex. *Nature* **546**, 118–123 (2017). doi:10.1038/nature22327 Medline

4. Y. Zhang, B. Sun, D. Feng, H. Hu, M. Chu, Q. Qu, J. T. Tarrasch, S. Li, T. Sun Kobilka, B. K. Kobilka, G. Skiniotis, Cryo-EM structure of the activated GLP-1 receptor in complex with a G protein. *Nature* **546**, 248–253 (2017). doi:10.1038/nature22394 Medline

5. L.-H. Zhao, S. Ma, I. Sutkeviciute, D.-D. Shen, X. E. Zhou, P. W. de Waal, C.-Y. Li, Y. Kang, L. J. Clark, F. G. Jean-Alphonse, A. D. White, D. Yang, A. Dai, X. Cai, J. Chen, C. Li, Y. Jiang, T. Watanabe, T. J. Gardella, K. Melcher, M.-W. Wang, J.-P. Vilardaga, H. E. Xu, Y. Zhang, Structure and dynamics of the active human parathyroid hormone receptor-1. *Science* **364**, 148–153 (2019). doi:10.1126/science.aav7942 Medline

6. G. Jiang, B. B. Zhang, Glucagon and regulation of glucose metabolism. *Am. J. Physiol. Endocrinol. Metab.* **284**, E671–E678 (2003). doi:10.1152/ajpendo.00492.2002 Medline

7. K. Hollenstein, C. de Graaf, A. Bortolato, M.-W. Wang, F. H. Marshall, R. C. Stevens, Insights into the structure of class B GPCRs. *Trends Pharmacol. Sci.* **35**, 12–22 (2014). doi:10.1016/j.tips.2013.11.001 Medline

8. L. J. Jelinek, S. Lok, G. B. Rosenberg, R. A. Smith, F. J. Grant, S. Biggs, P. A. Bensch, J. L. Kuijper, P. O. Sheppard, C. A. Sprecher, et, Expression cloning and signaling properties of the rat glucagon receptor. *Science* **259**, 1614–1616 (1993). doi:10.1126/science.8384375 Medline

9. K. E. Mayo, L. J. Miller, D. Bataille, S. Dalle, B. Göke, B. Thorens, D. J. Drucker, International Union of Pharmacology. XXXV. The glucagon receptor family. *Pharmacol. Rev.* **55**, 167–194 (2003). doi:10.1124/pr.55.1.6 Medline

10. T. D. Müller, B. Finan, C. Clemmensen, R. D. DiMarchi, M. H. Tschöp, The New Biology and Pharmacology of Glucagon. *Physiol. Rev.* **97**, 721–766 (2017). doi:10.1152/physrev.00025.2016 Medline

11. P. E. Cryer, S. N. Davis, H. Shamoon, Hypoglycemia in diabetes. *Diabetes Care* **26**, 1902–1912 (2003). doi:10.2337/diacare.26.6.1902 Medline

12. Y. M. Cho, C. E. Merchant, T. J. Kieffer, Targeting the glucagon receptor family for diabetes and obesity therapy. *Pharmacol. Ther.* **135**, 247–278 (2012). doi:10.1016/j.pharmthera.2012.05.009 Medline

13. J. H. Exton, G. A. Robison, E. W. Sutherland, C. R. Park, Studies on the role of adenosine 3′,5′-monophosphate in the hepatic actions of glucagon and catecholamines. *J. Biol. Chem.* **246**, 6166–6177 (1971). Medline

14. J. S. Pedersen, D. Dikov, J. L. Flink, H. A. Hjuler, G. Christiansen, D. E. Otzen, The changing face of glucagon fibrillation: Structural polymorphism and conformational imprinting. *J. Mol. Biol.* **355**, 501–523 (2006). doi:10.1016/j.jmb.2005.09.100 Medline

15. U. Hövelmann, B. V. Bysted, U. Mouritzen, F. Macchi, D. Lamers, B. Kronshage, D. V. Møller, T. Heise, Pharmacokinetic and pharmacodynamic characteristics of dasiglucagon, a novel soluble and stable glucagon analog. *Diabetes Care* **41**, 531–537 (2018). doi:10.2337/dc17-1402 Medline

16. C. G. Unson, Molecular determinants of glucagon receptor signaling. *Biopolymers* **66**, 218–235 (2002). doi:10.1002/bip.10259 Medline

17. H. Zhang, A. Qiao, L. Yang, N. Van Eps, K. S. Frederiksen, D. Yang, A. Dai, X. Cai, H. Zhang, C. Yi, C. Cao, L. He, H. Yang, J. Lau, O. P. Ernst, M. A. Hanson, R. C. Stevens, M.-W. Wang, S. Reedtz-Runge, H. Jiang, Q. Zhao, B. Wu, Structure of the glucagon receptor in complex with a glucagon analogue. *Nature* **553**, 106–110 (2018). doi:10.1038/nature25153 Medline

18. C. M. Koth, J. M. Murray, S. Mukund, A. Madjidi, A. Minn, H. J. Clarke, T. Wong, V. Chiang, E. Luis, A. Estevez, J. Rondon, Y. Zhang, I. Hötzel, B. B. Allan, Molecular basis for negative regulation of the glucagon receptor. *Proc. Natl. Acad. Sci. U.S.A.* **109**, 14393–14398 (2012). doi:10.1073/pnas.1206734109 Medline

19. H. Zhang, A. Qiao, D. Yang, L. Yang, A. Dai, C. de Graaf, S. Reedtz-Runge, V. Dharmarajan, H. Zhang, G. W. Han, T. D. Grant, R. G. Sierra, U. Weierstall, G. Nelson, W. Liu, Y. Wu, L. Ma, X. Cai, G. Lin, X. Wu, Z. Geng, Y. Dong, G. Song, P. R. Griffin, J. Lau, V. Cherezov, H. Yang, M. A. Hanson, R. C. Stevens, Q. Zhao, H. Jiang, M.-W. Wang, B. Wu, Structure of the full-length glucagon class B G-protein-coupled receptor. *Nature* **546**, 259–264 (2017). doi:10.1038/nature22363 Medline

20. D. Wootten, J. Simms, L. J. Miller, A. Christopoulos, P. M. Sexton, Polar transmembrane interactions drive formation of ligand-specific and signal pathway-biased family B G protein-coupled receptor conformations. *Proc. Natl. Acad. Sci. U.S.A.* **110**, 5211–5216 (2013). doi:10.1073/pnas.1221585110 Medline

21. C. G. Unson, D. Andreu, E. M. Gurzenda, R. B. Merrifield, Synthetic peptide antagonists of glucagon. *Proc. Natl. Acad. Sci. U.S.A.* **84**, 4083–4087 (1987). doi:10.1073/pnas.84.12.4083 Medline

22. C. G. Unson, E. M. Gurzenda, R. B. Merrifield, Biological activities of des-His1[Glu9]glucagon amide, a glucagon antagonist. *Peptides* **10**, 1171–1177 (1989). doi:10.1016/0196-9781(89)90010-7 Medline

23. C. G. Unson, D. Macdonald, K. Ray, T. L. Durrah, R. B. Merrifield, Position 9 replacement analogs of glucagon uncouple biological activity and receptor binding. *J. Biol. Chem.* **266**, 2763–2766 (1991). Medline

24. E. Dal Maso, Y. Zhu, V. Pham, C. A. Reynolds, G. Deganutti, C. A. Hick, D. Yang, A. Christopoulos, D. L. Hay, M.-W. Wang, P. M. Sexton, S. G. B. Furness, D. Wootten, Extracellular loops 2 and 3 of the calcitonin receptor selectively modify agonist binding and efficacy. *Biochem. Pharmacol.* **150**, 214–244 (2018). doi:10.1016/j.bcp.2018.02.005 Medline

25. F. Y. Siu, M. He, C. de Graaf, G. W. Han, D. Yang, Z. Zhang, C. Zhou, Q. Xu, D. Wacker, J. S. Joseph, W. Liu, J. Lau, V. Cherezov, V. Katritch, M.-W. Wang, R. C. Stevens, Structure of the human glucagon class B G-protein-coupled receptor. *Nature* **499**, 444–449 (2013). doi:10.1038/nature12393 Medline

26. C. de Graaf, G. Song, C. Cao, Q. Zhao, M.-W. Wang, B. Wu, R. C. Stevens, Extending the structural view of class B GPCRs. *Trends Biochem. Sci.* **42**, 946–960 (2017). doi:10.1016/j.tibs.2017.10.003 Medline

27. A. Glukhova, C. J. Draper-Joyce, R. K. Sunahara, A. Christopoulos, D. Wootten, P. M. Sexton, Rules of engagement: GPCRs and G proteins. *ACS Pharmacol. Transl. Sci.* **1**, 73–83 (2018). doi:10.1021/acsptsci.8b00026 Medline

28. Y. Du, N. M. Duc, S. G. F. Rasmussen, D. Hilger, X. Kubiak, L. Wang, J. Bohon, H. R. Kim, M. Wegrecki, A. Asuru, K. M. Jeong, J. Lee, M. R. Chance, D. T. Lodowski, B. K. Kobilka, K. Y. Chung, Assembly of a GPCR-G protein complex. *Cell* **177**, 1232–1242.e11 (2019). doi:10.1016/j.cell.2019.04.022 Medline

29. A. Manglik, A. C. Kruse, Structural Basis for G Protein-Coupled Receptor Activation. *Biochemistry* **56**, 5628–5634 (2017). doi:10.1021/acs.biochem.7b00747 Medline

30. G. G. Gregorio, M. Masureel, D. Hilger, D. S. Terry, M. Juette, H. Zhao, Z. Zhou, J. M. Perez-Aguilar, M. Hauge, S. Mathiasen, J. A. Javitch, H. Weinstein, B. K. Kobilka, S. C. Blanchard, Single-molecule analysis of ligand efficacy in β_2AR-G-protein activation. *Nature* **547**, 68–73 (2017). doi:10.1038/nature22354 Medline

31. F. J. Rojas, L. Birnbaumer, Regulation of glucagon receptor binding. Lack of effect of Mg and preferential role for GDP. *J. Biol. Chem.* **260**, 7829–7835 (1985). Medline

32. R. Seifert, U. Gether, K. Wenzel-Seifert, B. K. Kobilka, Effects of guanine, inosine, and xanthine nucleotides on β_2-adrenergic receptor/G_s interactions: Evidence for multiple receptor conformations. *Mol. Pharmacol.* **56**, 348–358 (1999). doi:10.1124/mol.56.2.348 Medline

33. A. Inoue, F. Raimondi, F. M. N. Kadji, G. Singh, T. Kishi, A. Uwamizu, Y. Ono, Y. Shinjo, S. Ishida, N. Arang, K. Kawakami, J. S. Gutkind, J. Aoki, R. B. Russell, Illuminating G-protein-coupling selectivity of GPCRs. *Cell* **177**, 1933–1947.e25 (2019). doi:10.1016/j.cell.2019.04.044 Medline

34. D. S. Serafin, N. R. Harris, N. R. Nielsen, D. I. Mackie, K. M. Caron, Dawn of a New RAMPage. *Trends Pharmacol. Sci.* **41**, 249–265 (2020). doi:10.1016/j.tips.2020.01.009 Medline

35. E. Lorenzen, T. Dodig-Crnković, I. B. Kotliar, E. Pin, E. Ceraudo, R. D. Vaughan, M. Uhlèn, T. Huber, J. M. Schwenk, T. P. Sakmar, Multiplexed analysis of the secretin-like GPCR-RAMP interactome. *Sci. Adv.* **5**, eaaw2778 (2019). doi:10.1126/sciadv.aaw2778 Medline

36. G. Jeschke, DEER distance measurements on proteins. *Annu. Rev. Phys. Chem.* **63**, 419–446 (2012). doi:10.1146/annurev-physchem-032511-143716 Medline

37. L. Sušac, M. T. Eddy, T. Didenko, R. C. Stevens, K. Wüthrich, A_{2A} adenosine receptor functional states characterized by ^{19}F-NMR. *Proc. Natl. Acad. Sci. U.S.A.* **115**, 12733–12738 (2018). doi:10.1073/pnas.1813649115 Medline

38. A. Manglik, T. H. Kim, M. Masureel, C. Altenbach, Z. Yang, D. Hilger, M. T. Lerch, T. S. Kobilka, F. S. Thian, W. L. Hubbell, R. S. Prosser, B. K. Kobilka, Structural insights into the dynamic process of β2-adrenergic receptor signaling. *Cell* **161**, 1101–1111 (2015). doi:10.1016/j.cell.2015.04.043 Medline

39. J. Okude, T. Ueda, Y. Kofuku, M. Sato, N. Nobuyama, K. Kondo, Y. Shiraishi, T. Mizumura, K. Onishi, M. Natsume, M. Maeda, H. Tsujishita, T. Kuranaga, M. Inoue, I. Shimada, Identification of a conformational equilibrium that determines the efficacy and functional selectivity of the μ-opioid receptor. *Angew. Chem. Int. Ed.* **54**, 15771–15776 (2015). doi:10.1002/anie.201508794 Medline

40. R. Sounier, C. Mas, J. Steyaert, T. Laeremans, A. Manglik, W. Huang, B. K. Kobilka, H. Déméné, S. Granier, Propagation of conformational changes during μ-opioid receptor activation. *Nature* **524**, 375–378 (2015). doi:10.1038/nature14680 Medline

41. L. M. Wingler, M. Elgeti, D. Hilger, N. R. Latorraca, M. T. Lerch, D. P. Staus, R. O. Dror, B. K. Kobilka, W. L. Hubbell, R. J. Lefkowitz, Angiotensin analogs with divergent bias stabilize distinct receptor conformations. *Cell* **176**, 468–478.e11 (2019). doi:10.1016/j.cell.2018.12.005 Medline

42. L. Ye, N. Van Eps, M. Zimmer, O. P. Ernst, R. S. Prosser, Activation of the A2A adenosine G-protein-coupled receptor by conformational selection. *Nature* **533**, 265–268 (2016). doi:10.1038/nature17668 Medline

43. J. F. Fay, D. L. Farrens, Purification of functional CB_1 and analysis by site-directed fluorescence labeling methods. *Methods Enzymol.* **593**, 343–370 (2017). doi:10.1016/bs.mie.2017.06.026 Medline

44. C. T. Schafer, J. F. Fay, J. M. Janz, D. L. Farrens, Decay of an active GPCR: Conformational dynamics govern agonist rebinding and persistence of an active, yet empty, receptor state. *Proc. Natl. Acad. Sci. U.S.A.* **113**, 11961–11966 (2016). doi:10.1073/pnas.1606347113 Medline

45. X. J. Yao, G. Vélez Ruiz, M. R. Whorton, S. G. F. Rasmussen, B. T. DeVree, X. Deupi, R. K. Sunahara, B. Kobilka, The effect of ligand efficacy on the formation and stability of a GPCR-G protein complex. *Proc. Natl. Acad. Sci. U.S.A.* **106**, 9501–9506 (2009). doi:10.1073/pnas.0811437106 Medline

46. R. O. Dror, D. H. Arlow, P. Maragakis, T. J. Mildorf, A. C. Pan, H. Xu, D. W. Borhani, D. E. Shaw, Activation mechanism of the β2-adrenergic receptor. *Proc. Natl. Acad. Sci. U.S.A.* **108**, 18684–18689 (2011). doi:10.1073/pnas.1110499108 Medline

47. T. M. Gupte, M. Ritt, M. Dysthe, R. U. Malik, S. Sivaramakrishnan, Minute-scale persistence of a GPCR conformation state triggered by non-cognate G protein interactions primes signaling. *Nat. Commun.* **10**, 4836 (2019). doi:10.1038/s41467-019-12755-9 Medline

48. C. P. Kimball, J. R. Murlin, Aqueous extracts of pancreas III. Some precipitation reactions of insulin. *J. Biol. Chem.* **58**, 337–346 (1923).

49. Y. Yin, P. W. de Waal, Y. He, L.-H. Zhao, D. Yang, X. Cai, Y. Jiang, K. Melcher, M.-W. Wang, H. E. Xu, Rearrangement of a polar core provides a conserved mechanism for constitutive activation of class B G protein–coupled receptors. *J. Biol. Chem.* **292**, 9865–9881 (2017). doi:10.1074/jbc.M117.782987 Medline

50. S. G. F. Rasmussen, B. T. DeVree, Y. Zou, A. C. Kruse, K. Y. Chung, T. S. Kobilka, F. S. Thian, P. S. Chae, E. Pardon, D. Calinski, J. M. Mathiesen, S. T. A. Shah, J. A. Lyons, M. Caffrey, S. H. Gellman, J. Steyaert, G. Skiniotis, W. I. Weis, R. K. Sunahara, B. K. Kobilka, Crystal structure of the β2 adrenergic receptor-Gs protein complex. *Nature* **477**, 549–555 (2011). doi:10.1038/nature10361 Medline

51. A. Koehl, H. Hu, D. Feng, B. Sun, Y. Zhang, M. J. Robertson, M. Chu, T. S. Kobilka, T. Laeremans, J. Steyaert, J. Tarrasch, S. Dutta, R. Fonseca, W. I. Weis, J. M. Mathiesen, G. Skiniotis, B. K. Kobilka, Structural insights into the activation of metabotropic glutamate receptors. *Nature* **566**, 79–84 (2019). doi:10.1038/s41586-019-0881-4 Medline

52. D. P. Staus, L. M. Wingler, M. Choi, B. Pani, A. Manglik, A. C. Kruse, R. J. Lefkowitz, Sortase ligation enables homogeneous GPCR phosphorylation to reveal diversity in β-arrestin coupling. *Proc. Natl. Acad. Sci. U.S.A.* **115**, 3834–3839 (2018). doi:10.1073/pnas.1722336115 Medline

53. S. Q. Zheng, E. Palovcak, J.-P. Armache, K. A. Verba, Y. Cheng, D. A. Agard, MotionCor2: Anisotropic correction of beam-induced motion for improved cryo-electron microscopy. *Nat. Methods* **14**, 331–332 (2017). doi:10.1038/nmeth.4193 Medline

54. K. Zhang, Gctf: Real-time CTF determination and correction. *J. Struct. Biol.* **193**, 1–12 (2016). doi:10.1016/j.jsb.2015.11.003 Medline

55. J. Zivanov, T. Nakane, B. O. Forsberg, D. K. Elife, 2018, New tools for automated high-resolution cryo-EM structure determination in RELION-3. *eLife* **7**, e42166 (2018).

56. T. Grant, A. Rohou, N. G. Elife, 2018, cisTEM, user-friendly software for single-particle image processing. *eLife* **7**, e35383 (2018).

57. J. B. Heymann, Guidelines for using Bsoft for high resolution reconstruction and validation of biomolecular structures from electron micrographs. *Protein Sci.* **27**, 159–171 (2018). doi:10.1002/pro.3293 Medline

58. E. F. Pettersen, T. D. Goddard, C. C. Huang, G. S. Couch, D. M. Greenblatt, E. C. Meng, T. E. Ferrin, UCSF Chimera—A visualization system for exploratory research and analysis. *J. Comput. Chem.* **25**, 1605–1612 (2004). doi:10.1002/jcc.20084 Medline

59. P. Emsley, K. Cowtan, *Coot*: Model-building tools for molecular graphics. *Acta Crystallogr. D Biol. Crystallogr.* **60**, 2126–2132 (2004). doi:10.1107/S0907444904019158 Medline

60. P. D. Adams, P. V. Afonine, G. Bunkóczi, V. B. Chen, N. Echols, J. J. Headd, L.-W. Hung, S. Jain, G. J. Kapral, R. W. Grosse Kunstleve, A. J. McCoy, N. W. Moriarty, R. D. Oeffner, R. J. Read, D. C. Richardson, J. S. Richardson, T. C. Terwilliger, P. H. Zwart, The Phenix software for automated determination of macromolecular structures. *Methods* **55**, 94–106 (2011). doi:10.1016/j.ymeth.2011.07.005 Medline

61. C. J. Williams, J. J. Headd, N. W. Moriarty, M. G. Prisant, L. L. Videau, L. N. Deis, V. Verma, D. A. Keedy, B. J. Hintze, V. B. Chen, S. Jain, S. M. Lewis, W. B. Arendall 3rd, J. Snoeyink, P. D. Adams, S. C. Lovell, J. S. Richardson, D. C. Richardson, MolProbity: More and better reference data for improved all-atom structure validation. *Protein Sci.* **27**, 293–315 (2018). doi:10.1002/pro.3330 Medline

62. M. Pannier, S. Veit, A. Godt, G. Jeschke, H. W. Spiess, Dead-time free measurement of dipole-dipole interactions between electron spins. *J. Magn. Reson.* **142**, 331–340 (2000). doi:10.1006/jmre.1999.1944 Medline

63. Y. Polyhach, E. Bordignon, R. Tschaggelar, S. Gandra, A. Godt, G. Jeschke, High sensitivity and versatility of the DEER experiment on nitroxide radical pairs at Q-band frequencies. *Phys. Chem. Chem. Phys.* **14**, 10762–10773 (2012). doi:10.1039/c2cp41520h Medline

64. G. Jeschke, V. Chechik, P. Ionita, A. Godt, H. Zimmermann, J. Banham, C. R. Timmel, D. Hilger, H. Jung, DeerAnalysis2006—A comprehensive software package for analyzing pulsed ELDOR data. *Appl. Magn. Reson.* **30**, 473–498 (2006). doi:10.1007/BF03166213

65. W. Humphrey, A. Dalke, K. Schulten, VMD: Visual molecular dynamics. *J. Mol. Graph.* **14**, 33–38, 27–28 (1996). doi:10.1016/0263-7855(96)00018-5 Medline

66. J. C. Phillips, R. Braun, W. Wang, J. Gumbart, E. Tajkhorshid, E. Villa, C. Chipot, R. D. Skeel, L. Kalé, K. Schulten, Scalable molecular dynamics with NAMD. *J. Comput. Chem.* **26**, 1781–1802 (2005). doi:10.1002/jcc.20289 Medline

67. J. Huang, S. Rauscher, G. Nawrocki, T. Ran, M. Feig, B. L. de Groot, H. Grubmüller, A. D. MacKerell Jr., CHARMM36m: An improved force field for folded and intrinsically disordered proteins. *Nat. Methods* **14**, 71–73 (2017). doi:10.1038/nmeth.4067 Medline

68. T. Darden, D. York, L. Pedersen, Particle mesh Ewald: An N·log(N) method for Ewald sums in large systems. *J. Chem. Phys.* **98**, 10089–10092 (1998). doi:10.1063/1.464397

69. S. E. Feller, Y. Zhang, R. W. Pastor, B. R. Brooks, Constant pressure molecular dynamics simulation: The Langevin piston method. *J. Chem. Phys.* **103**, 4613–4621 (1998). doi:10.1063/1.470648

70. G. J. Martyna, Remarks on "Constant-temperature molecular dynamics with momentum conservation". *Phys. Rev. E Stat. Phys. Plasmas Fluids Relat. Interdiscip. Topics* **50**, 3234–3236 (1994). doi:10.1103/PhysRevE.50.3234 Medline

71. J.-P. Ryckaert, G. Ciccotti, H. J. C. Berendsen, Numerical integration of the cartesian equations of motion of a system with constraints: Molecular dynamics of n-alkanes. *J. Comput. Phys.* **23**, 327–341 (1977). doi:10.1016/0021-9991(77)90098-5

72. T. D. Goddard, C. C. Huang, E. C. Meng, E. F. Pettersen, G. S. Couch, J. H. Morris, T. E. Ferrin, UCSF ChimeraX: Meeting modern challenges in visualization and analysis. *Protein Sci.* **27**, 14–25 (2018). doi:10.1002/pro.3235 Medline

73. X. Liu, X. Xu, D. Hilger, P. Aschauer, J. K. S. Tiemann, Y. Du, H. Liu, K. Hirata, X. Sun, R. Guixà-González, J. M. Mathiesen, P. W. Hildebrand, B. K. Kobilka, Structural insights into the process of GPCR-G protein complex Formation. *Cell* **177**, 1243–1251.e12 (2019). doi:10.1016/j.cell.2019.04.021 Medline